

Article

Study of the Synergistic Effect of Induction Heating Parameters on Heating Efficiency Using Taguchi Method and Response Surface Method

Jiajie Li , Peng Zhang, Jinlan Hu and Yanfei Zhang * 

School of Materials Science and Engineering, North University of China, Taiyuan 030051, China

* Correspondence: zhangyanfei208@sina.com

Abstract: This work designed an intercalation internal induction heating coil in a mold and drew a plate-type steel for the heating mold (size: 300 mm × 200 mm × 40 mm). First, to explore the influence rule of special-shaped coils on induction heating effects, the temperature rise curve on the mold surface was simulated at different heating depths, currents, and frequencies. Next, the extent to which these three factors affect the maximum mean temperature and temperature uniformity was discussed using the Taguchi method and the analysis of variance (ANOVA). Results show that heating depth and current are important factors influencing the target results, while frequency only has a small impact. The maximum mean temperature reaches its peak level when the heating depth, current, and frequency are at the respective values of 5 mm, 1200 A, and 40 KHz and the optimal temperature uniformity can be achieved when these values are 7 mm, 800 A, and 20 KHz, respectively. Finally, the synergistic effect of different factors on target results was analyzed using the response surface method (RSM).

Keywords: induction heating; numerical simulation; Taguchi method; ANOVA; RSM



Citation: Li, J.; Zhang, P.; Hu, J.; Zhang, Y. Study of the Synergistic Effect of Induction Heating Parameters on Heating Efficiency Using Taguchi Method and Response Surface Method. *Appl. Sci.* **2023**, *13*, 555. <https://doi.org/10.3390/app13010555>

Academic Editor: Adrian Irimescu

Received: 8 December 2022

Revised: 24 December 2022

Accepted: 28 December 2022

Published: 30 December 2022



Copyright: © 2022 by the authors. Licensee MDPI, Basel, Switzerland. This article is an open access article distributed under the terms and conditions of the Creative Commons Attribution (CC BY) license (<https://creativecommons.org/licenses/by/4.0/>).

1. Introduction

The flourishing 3C industry has made people pay more attention to the appearance of plastic products. Traditionally, after injection molding, products are usually subjected to high gloss treatment as affected by the mold temperature and output efficiency of the product [1,2]. In recent years, the rapid heating cycle molding (RHCM) has greatly raised the upper limit of the mold temperature while maintaining output efficiency, giving a high glossed surface to the product after demolding with the high gloss mold [3–5]. Based on different heating methods, RHCM technology can be divided into steam heating RHCM, electric heating RHCM, and induction heating RHCM. Due to the restricted, limited help of steam heating in increasing mold temperature, electric heating was developed, which is able to greatly build up the mold surface temperature yet with a relatively slow heating speed and high energy consumption. Wada et al. [6] first proposed in 1982 to use electromagnetic induction to heat the mold cavity wall and studied the influence of output power, frequency, and other parameters on the heating speed. Murata et al. [7] designed an injection molding machine that is able to control the melt flow and induction heating and used it to produce the carbon fiber-reinforced semi-aromatic polyamide. They found that by elevating the mold heating temperature, the weld lines could be avoided, and the surface quality and bending strength of products could be improved. Fu et al. [8] developed an induction heating device for hot embossing and made the mold out of nickel, which enhanced the heating rate of nanoimprint lithography. The results showed that it could be printed onto a 4-inch polymer sheet within 5 min. Muszyński et al. [9] applied the induction heating device to injection molding to improve the mechanical properties of elastic hinges. As indicated by test results, the rigidity, tensile strength, and elongation at the break of these hinges were significantly enhanced. Poszwa et al. [10] investigated the effect of induction

heating on the strength characteristics of flexible hinges by using induction heating RHCM molding technology to manufacture thin layer hinges, showing that the mold temperature rose to 187 °C at a heating time of 2.5 s. Increasing the mold temperature using induction heating increased the strength of the upper hinge by 45% and the lower hinge by 65%. Minh et al. [11] used a dynamic mold temperature control system to improve the flow length of the melt. The authors used an external spiral coil to heat the cavity surface and showed that the mold heating rate decreased as the heating distance increased, but that the use of induction heating injection molding techniques resulted in an increase in melt flow length and fill rate.

To sum up, induction heating is superior in molding polymer materials, and the heating efficiency has become a research focus to meet the requirement for higher industrial production efficiency. Many scholars have studied the effects of various induction heating parameters, such as current, temperature, frequency, power, and heating depth, on heating efficiency. To explore the impact of these parameters on heating quality, Omarova et al. [12] carried out numerical simulation and experimental research using two kinds of induction devices, thus revealing the configuration of the inductor and achieving the most uniform heating of workpieces. Thuan et al. [13] applied the internal induction heater to injection molding and found through simulations and experiments that the mold temperature increased from 30 °C to 180 °C within 9 s, showing a heating rate of up to 16 °C/s, and the melt flow length was significantly improved. The experimental results were in line with simulation ones. Xiao et al. [14] proposed a new rapid heat cycle molding technology for internal induction heating and optimized the induction heating system by multipurpose optimal method in respect of the current, frequency, layout, and clearance of induction coils. Finally, they verified the effectiveness of this technology with the car spoiler as a model.

The conventional spiral-shaped induction heating coil is mostly used in the induction heating RHCM throughout its development, which is disadvantaged by the low mold temperature at the spiral center of the coil and poor uniformity of the mold surface temperature despite its high heating efficiency. With this in mind, an intercalation internal induction heating coil is designed to simulate the temperature distribution on the mold surface with different mold materials [15–17]. The multiphysics simulation software is used to characterize the results. The new induction heating coil is different from the traditional spiral coil, this soft coil is interspersed inside the mold, which is able to solve the shortcomings of the spiral coil center low temperature zone, and the use of soft coil can improve the coil inside the mold with the shape, so that the mold temperature distribution is more uniform. In addition, whether the influence of current, frequency, and heating depth on the heating efficiency is consistent with previous research during the induction heating of this new coil is verified. However, in most existing studies, the extent to which the parameters affect the results is not mentioned and the synergistic effect of any two parameters on these results is not discussed. Therefore, this extent and effect were explored herein using Taguchi method and response surface method (RSM). Taguchi method uses orthogonal tables to design experiments that can be made larger to replace the whole with a partial experimental design that can greatly reduce the pressure on the computer to run, while using RSM can reflect the interaction between the two factors more intuitively than single factor experiments and provide a theoretical range for selecting the optimal value of the factors.

2. Research Methods

2.1. Multiphysics Simulation

The simulation analysis of electromagnetic induction heating involves the multiphysics coupling analysis of the electromagnetic heating [18], in which the analysis of the electromagnetic field is based on Maxwell field equations summarized by Maxwell in the 19th century, including Gaussian law (1), Gaussian electromagnetic induction law (2), the

Faraday law of electromagnetic induction (3), and the Ampere circuit law (4) [19]. The differential form is as follows:

$$\nabla \cdot \mathbf{D} = \rho \quad (1)$$

$$\nabla \cdot \mathbf{B} = 0 \quad (2)$$

$$\nabla \times \mathbf{E} = -\frac{\partial \mathbf{B}}{\partial t} \quad (3)$$

$$\nabla \times \mathbf{H} = \mathbf{J} + \frac{\partial \mathbf{D}}{\partial t} \quad (4)$$

In the above equations, \mathbf{D} represents the electric flux density, C/m^2 ; \mathbf{B} is magnetic flux density, T; \mathbf{E} is electric field strength, V/m; \mathbf{H} is magnetic field strength, A/m; \mathbf{J} is conduction current, A; t is time, s; and ρ is the charge density, C/m^3 .

Of these, \mathbf{D} , \mathbf{H} , and \mathbf{J} can form the constitutive equation together with the dielectric constant ϵ (F/m), magnetic permeability μ (H/m), and electric conductivity σ (S/m) of electromagnetic material properties as follows:

$$\mathbf{D} = \epsilon \mathbf{E} \quad (5)$$

$$\mathbf{B} = \mu \mathbf{H} \quad (6)$$

$$\mathbf{J} = \sigma \mathbf{E} \quad (7)$$

The heat transfer phenomenon occurring in induction heating is the heat conduction in the conductor, which can be expressed by the transient heat conduction Equation (8) used for all simulations as follows:

$$\rho C_p \frac{\partial T}{\partial t} = k \nabla^2 T + Q \quad (8)$$

In this formula, T refers to temperature, K; ρ is density, kg/m^3 ; C_p is the specific heat capacity, $J/(kg \cdot K)$; k is the thermal conductivity of the material, $W/(m \cdot K)$; and Q is Joule heat, J.

To obtain a simplified calculation model, CATIA software was used to draw the plate-type steel for the heating mold with a mold size of $300 \text{ mm} \times 200 \text{ mm} \times 40 \text{ mm}$. In addition, COMSOL Multiphysics software was introduced to simulate the mold surface temperature distribution and heating rate under three different conditions. A specific parameter range was set for a 30 KW induction heating power supply, with a maximum current of 1400 A when the equipment was running at full power, and a safety margin was set so that the current parameter was set to a maximum of 1200 A. As the induction coils needed to be fitted as close to the mold surface as possible, 5 mm to 9 mm was the ideal range to balance the heating effect with the mold structure. High frequency induction heating required an inductor frequency of 10 KHz or more, while a 30 KW induction heating power supply was set to a maximum regulation frequency of 50 KHz, so the frequency range was 20 KHz to 40 KHz. The parameters are set as follows: (1) The depths from the coil to the mold surface were set to be 5 mm, 7 mm, and 9 mm, respectively, to explore the influence of varying depths on the uniformity of the temperature distribution on the mold surface and the heating rate. The two-dimensional diagram of the mold is shown in Figure 1a. As the inductors are made of soft coils and need to be mounted inside the mold, they need to be perforated inside the mold. This is the reason for using soft coils as inductors, which can be arranged at random inside the mold and reach the desired temperature of the mold. (2) The impact of different currents on the heating efficiency of the new induction heating coil was studied at following currents: 800 A, 1000 A, and 1200 A. (3) The frequencies were set to 20 KHz, 30 KHz, and 40 KHz, respectively, to discuss the effect of varying frequencies on this efficiency.

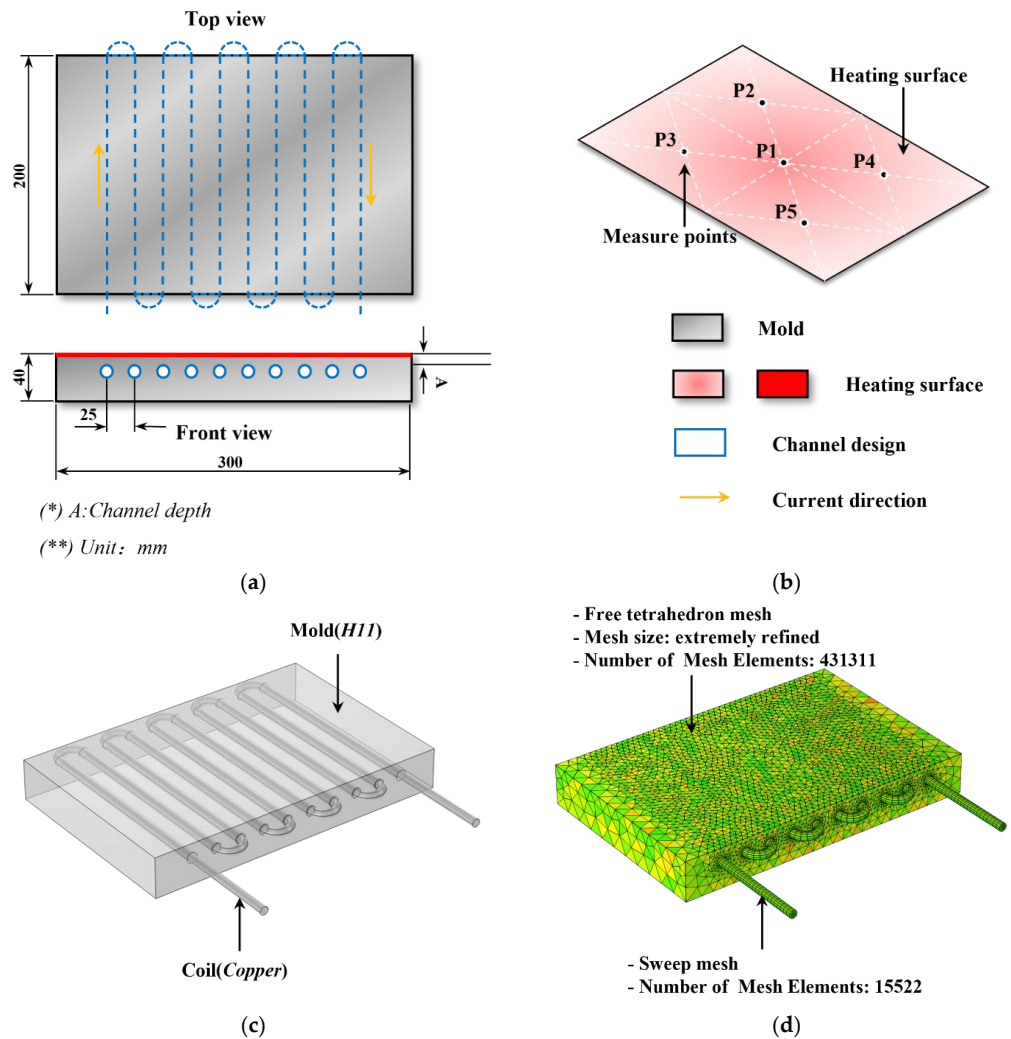


Figure 1. Mold model drawing and temperature measure points: (a) mold size drawing; (b) temperature measure points; (c) mold 3D model drawing; (d) mesh division drawing.

The temperature of 5 measuring points on the mold surface, as shown in Figure 1b, was selected as the final result and the reference temperature of the mold surface. After heating for 30 s, the final temperature at these 5 points was obtained, and their mean temperature was calculated using Equation (9) and regarded as the final heating temperature of the mold. Figure 1c shows a perspective view of the 3D simulation model with the induction coil interspersed in the interior of the mold, and Figure 1d shows the mesh division. The focus of this simulation was to characterize the temperature distribution on the surface of the mold, therefore a very fine free tetrahedral mesh was used for the mold and, for the coil, a swept mesh with 15522 mesh elements was used, which reduces the pressure on the calculation run and speeds up the calculation time. The overall experimental scheme is shown in Table 1.

$$\bar{x} = \frac{1}{n} \sum_{i=1}^n x_i \tag{9}$$

In this equation, \bar{x} represents the mean temperature of 5 points; x_i is the final heating temperature of each point; and n refers to the number of measuring points, which is set to be 5 in this experiment.

In this electromagnetic thermal multiphysics coupling, the low mold temperature has little influence on the mold material parameters even after it rises, the influence of which on the material parameters can be ignored as a result. The heat transfer mode of all external surfaces of the mold is set to free convection with air, the ambient temperature is 20 °C,

and the heat transfer coefficient is $10 \text{ W}/(\text{m}^2 \cdot \text{K})$. The parameters of other air, mold, and induction coils are shown in Table 2, where μ_r is a relative dielectric constant; σ represents the electric conductivity; ρ refers to the density; K is the electric conductivity; and C_p is the heat capacity at constant pressure. The air and copper parameters are sourced from the COMSOL software's own material library and H11 from Roctool's actual mold parameters.

Table 1. Simulation experiment scheme of induction heating.

| Scheme | Channel Depth/mm | Current/A | Frequency/KHz |
|--------|------------------|-----------|---------------|
| A1 | 5 | 1000 | 30 |
| A2 | 7 | 1000 | 30 |
| A3 | 9 | 1000 | 30 |
| B1 | 9 | 800 | 30 |
| B2 | 9 | 1200 | 30 |
| C1 | 9 | 1000 | 20 |
| C2 | 9 | 1000 | 40 |

Table 2. Material parameters.

| Material | μ_r (-) | σ (S/m) | ρ (kg/m ³) | K (W/(m·K)) | C_p (J/kg·K) |
|-------------|-------------|-------------------|-----------------------------|---------------|----------------|
| Air | 1 | 1 | 1.18 | 0.025 | 1005 |
| Copper | 1 | 5.9×10^7 | 8960 | 400 | 385 |
| H11(1.2343) | 55 | 10^7 | 7700 | 45 | 460 |

2.2. Taguchi Method and ANOVA

The Taguchi method, which was proposed by Dr. Genichi Taguchi of Japan, introduces the orthogonal table into experimental designs. It spread quickly around the world due to multiple advantages, including a high reproducibility of experimental results, a scalability of configuration experiments, a lower number of tests, simple operation, and easy configuration. Using this method, the optimal parameter combination under corresponding horizontal conditions can be realized through some experiments. In this study, the heating depth, current, and frequency were selected as parameters to carry out simulation experiments based on the L9 orthogonal table involving three factors and three levels that was designed by Taguchi method. Table 3 presents the levels of three factors. The specific experimental design is shown in Table 4. Finally, the experimental results were first analyzed based on the signal-to-noise (S/N) ratio and then divided by optimization objectives into three characteristics: nominal-the-best, larger-the-better, and smaller-the-better [20], which correspond to Equation (10), Equation (11), and Equation (12), respectively:

$$\frac{\text{Signal}}{\text{Noise}} = -10 \log_{10} \left(\frac{\mu^2(n-1)}{\sum_{i=1}^n (y_i - \mu)^2} \right) \quad (10)$$

$$\frac{\text{Signal}}{\text{Noise}} = -10 \log_{10} \frac{1}{n} \sum_{i=1}^n \frac{1}{y_i^2} \quad (11)$$

$$\frac{\text{Signal}}{\text{Noise}} = -10 \log_{10} \frac{1}{n} \sum_{i=1}^n y_i^2 \quad (12)$$

Table 3. Levels of experimental factors.

| Level of Factors | Experimental Factors | | |
|------------------|----------------------|---------------|-------------------|
| | (A) Depth/mm | (B) Current/A | (C) Frequency/KHz |
| 1 | 5 | 800 | 20 |
| 2 | 7 | 1000 | 30 |
| 3 | 9 | 1200 | 40 |

Table 4. Design of the L9 orthogonal experiment.

| No. | A | B | C |
|-----|---|------|----|
| 1 | 5 | 800 | 20 |
| 2 | 5 | 1000 | 30 |
| 3 | 5 | 1200 | 40 |
| 4 | 7 | 800 | 30 |
| 5 | 7 | 1000 | 40 |
| 6 | 7 | 1200 | 20 |
| 7 | 9 | 800 | 40 |
| 8 | 9 | 1000 | 20 |
| 9 | 9 | 1200 | 30 |

In the above equations, n represents the number of experiments in each group; y_i refers to the results of a single experiment; and μ is the sample mean. It is necessary in this experiment that the higher the mean temperature after heating, the better, which is classified into the larger-the-better characteristic. The range of temperature at five points, denoted by s , is calculated with Equation (13) and is used to characterize the temperature uniformity:

$$s = y_{\max} - y_{\min} \tag{13}$$

where s represents the range of temperature at measuring points; y_{\max} and y_{\min} are maximum and minimum temperatures of these five points, respectively. Then, the extent to which each factor affects the experimental results is determined through the analysis of variance (ANOVA).

2.3. Response Surface Method

The RSM analysis is used to optimize and evaluate the experimental data and determine the relationship between the two parameters and analysis results. Using this method, the ultimate relationship can be presented by response surface diagrams, in which the optimal response value is identified and its regression equation is calculated with Equation (14) [21]:

$$Y = a_0 + \sum_{i=1}^k a_i x_i + \sum_{i=1}^k a_{ii} x_i x_i + \sum_{ij}^k a_{ij} x_i x_j \tag{14}$$

where Y is the response output, which refers to the maximum mean temperature and the range of temperature in this study, and x and k represent the level and number of factors, respectively.

3. Results and Discussion

3.1. Results of Multiphysics Simulation

In previous studies, the induction heating depth, current, and frequency were usually analyzed using spiral-shaped coils, without specifying the effects of special-shaped ones on conclusions. Therefore, these factors are researched and compared in this section to verify whether related conclusions are followed. To explore the influence of different parameters on results, the depth was set to be 5 mm, 7 mm, and 9 mm, respectively; the current was set to 800 A, 1000 A, and 1200 A, respectively; and the frequency was set to 20 KHz, 30 KHz, and 40 KHz, respectively. As shown in Figure 2a, while the mold surface temperature rise

rate was 2.3 °C/s when the coil is 5 mm from the surface, it gradually decreased to 2.1 °C/s and to 1.9 °C/s when the depth expanded to 7 mm and to 9 mm. The small depth gradient means the temperature rise rate decreases slightly. According to the temperature rise curves at different currents in Figure 2b, the temperature rise rate accelerates significantly at higher currents. When the current increases from 800 A to 1200 A, this rate rises from 1.2 °C/s to 2.6 °C/s. The temperature rise curves at varying frequencies are presented in Figure 2c. It can be seen that there is little difference among these curves due to the small gradient of this parameter. However, the partial enlarged view shows that the temperature rise rate increases with the frequency. In summary, the temperature rise rate of induction heating increases with increased currents and frequencies but decreases with the increase of heating depth, which is consistent with correlating studies [22] and is in accordance with the principles of heat transfer and Joule heating. As the current increases, the heating power of the power supply increases and the heating rate of the mold increases significantly. As the coil frequency increases, the skin effect of the current becomes stronger and the mold heats up faster. However, as the heating depth increases, the heat transfer distance of the mold also increases and the heat loss becomes more and more serious, so the heating rate of the mold surface decreases as the heating depth increases. The temperature distribution nephogram of the mold surface after being heated for 30 s under different conditions is shown in Figure 3.

3.2. Results of the Taguchi Method and ANOVA

Table 5 exhibits the simulated data of the maximum mean temperature and temperature uniformity in each group of experiments and their respective S/N ratios. Figure 4 shows the main effects plots for means and S/N ratios of three factors. The factors' magnitude of influence is determined by the difference between the maximum and minimum S/N ratios: the larger the difference, the greater the influence. As presented in Figure 4a, the temperature uniformity was most affected by heating depth and then by current and frequency successively. It first rose and then declined as the heating depth extended. It first decreased and then increased with rising frequency. It reduces as the current increases. At this level of factors, the optimal temperature uniformity was achieved at a heating depth of 7 mm, a current of 800 A, and a frequency of 20 KHz.

Figure 4b illustrates the extent to which the three parameters affect the maximum mean temperature. It can be found that this temperature rises with the decrease of heating depth and the increase of current and frequency. In other words, the maximum mean temperature is negatively correlated with heating depth but is positively correlated with current and frequency. In respect to this temperature, the optimal combination of these parameters is as follows: the heating depth is 5 mm; the current is 1200 A; and the frequency is 40 KHz. Table 6 describes the ANOVA of each factor based on the 95% confidence interval (CI), which is used to evaluate how much each factor influences the maximum mean temperature and temperature uniformity. In this analysis, the P value of less than 0.05 means the factor is an important one affecting the target results [23]. It is observed from Table 6 that the maximum mean temperature is most affected by current, with a contribution rate of 95.54%, which is followed by heating depth with a contribution rate of 4.17%, while frequency has little impact on this temperature, showing a contribution rate of 0.29%. Therefore, the influence extent of current is much higher than that of the other two factors. By contrast, the heating depth is the most important factor affecting the temperature uniformity, showing a contribution rate of 59.59%. It is followed by the current with a contribution rate of 40.18% and then by the frequency with a contribution rate of 0.23%. Among them, heating depth and current are principal factors influencing the temperature uniformity, while the impact of frequency is negligible. To sum up, the target values are significantly affected by heating depth and current, with their influence extents much higher than that of the frequency. The percentage for the contribution rates of different factors is presented in Figure 5.

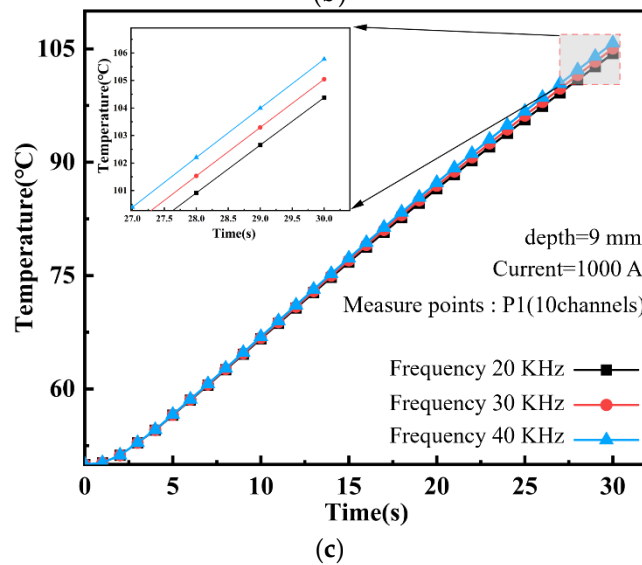
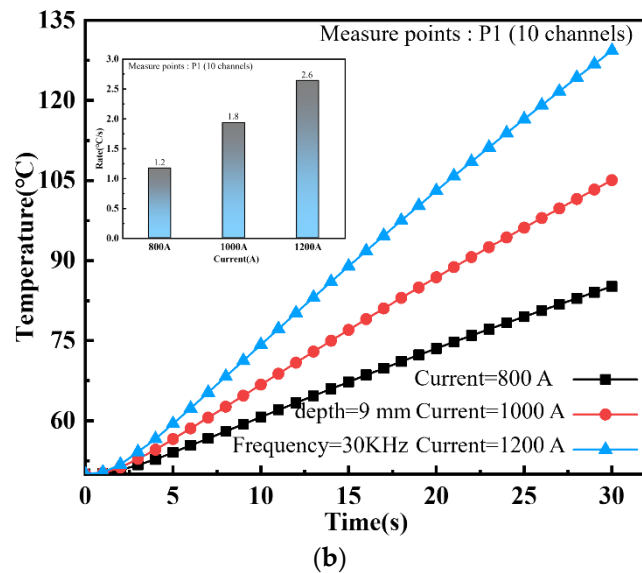
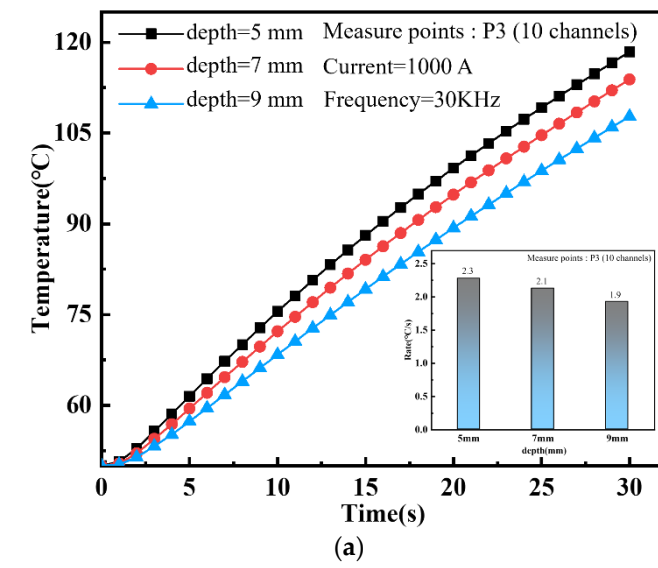


Figure 2. Temperature rise curve under different parameters: (a) depth, (b) current, (c) frequency.

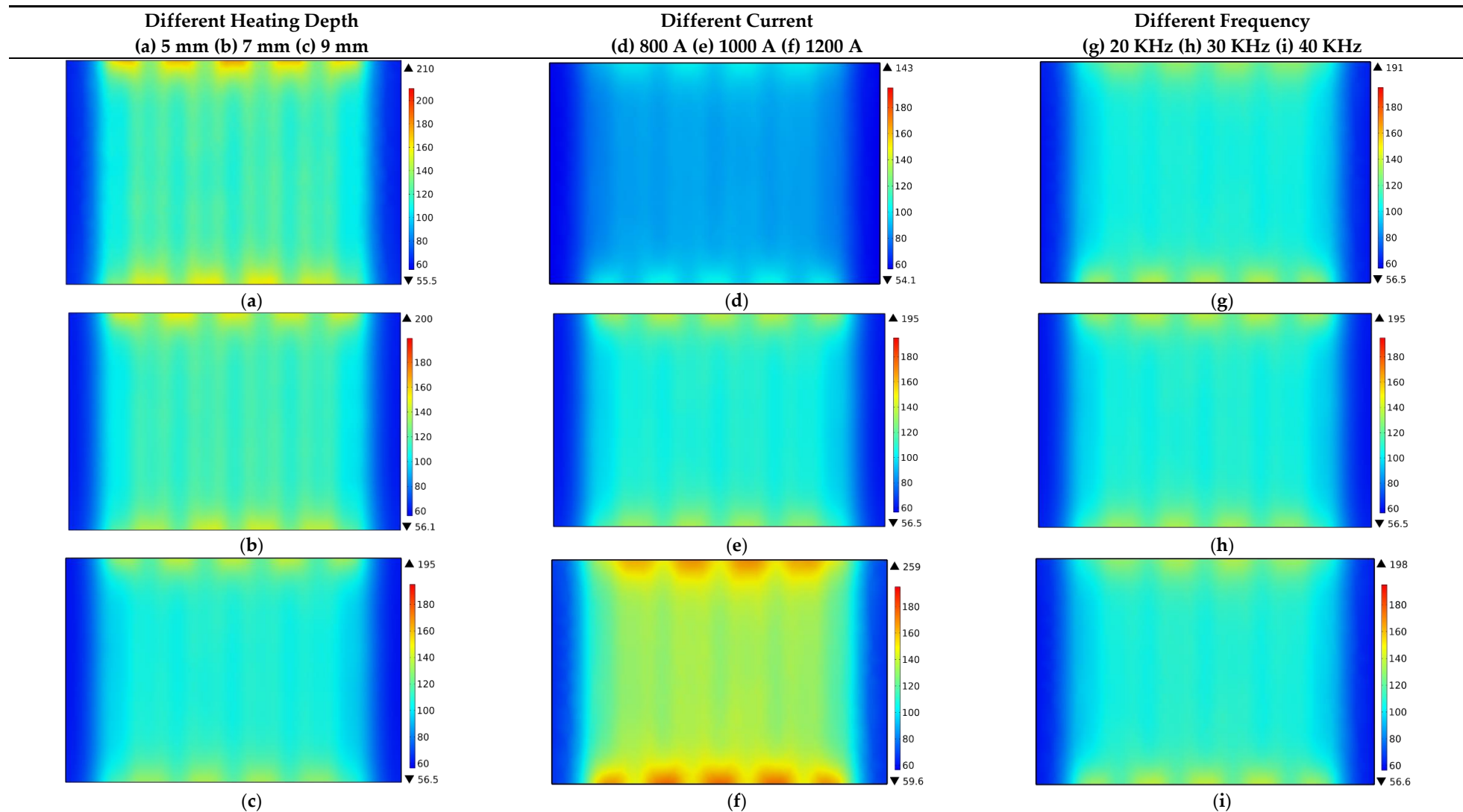


Figure 3. Temperature distribution nephograms on the mold surface under different parameters.

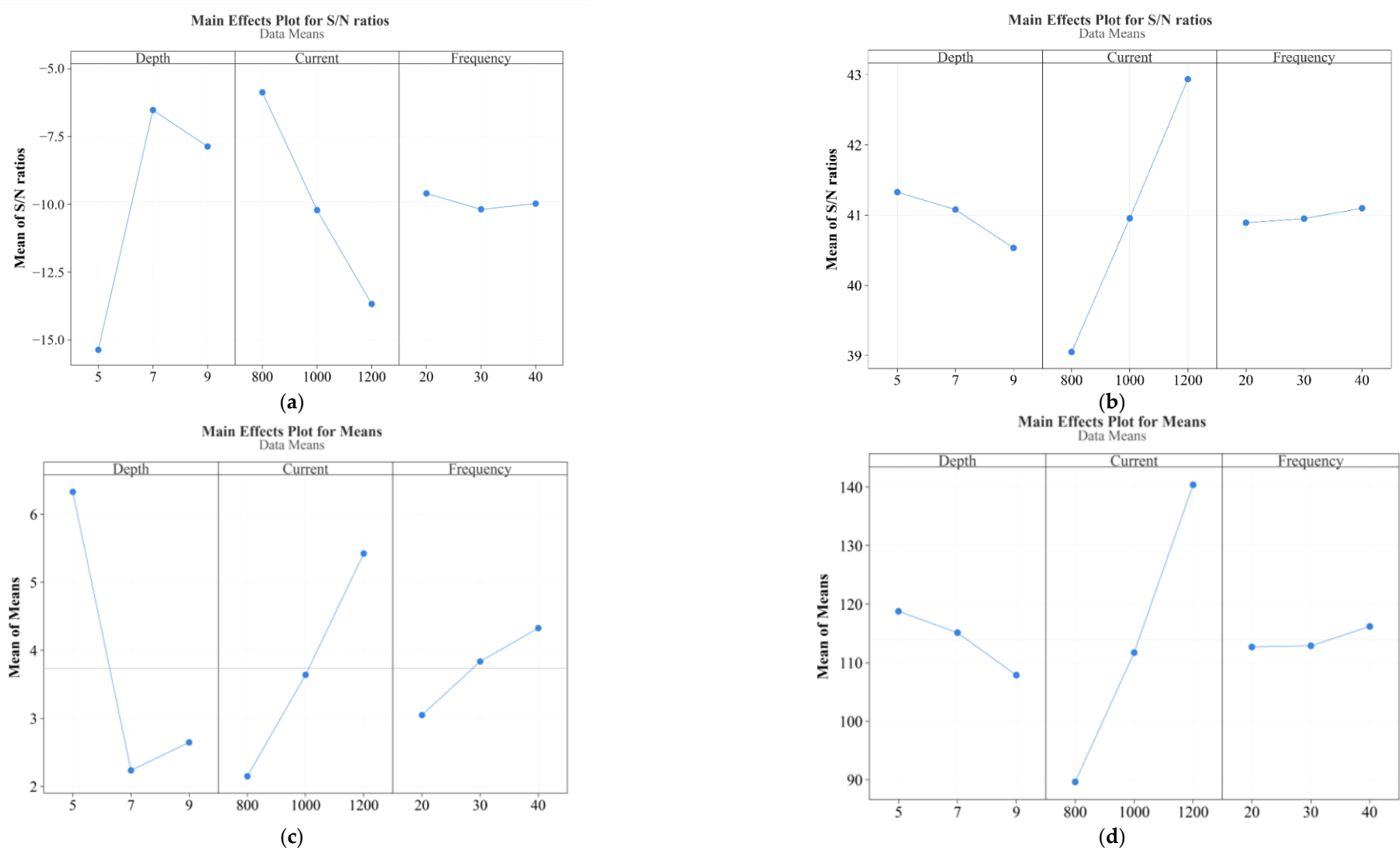


Figure 4. Main effects plots in the Taguchi experiment: (a) main effects plot for S/N ratios of three factors in respect of temperature uniformity; (b) main effects plot for S/N ratios of three factors in respect of max. mean temperature; (c) main effects plot for means of three factors in respect of temperature uniformity; (d) main effects plot for means of three factors in respect of max. mean temperature.

Table 5. Simulation results and S/N ratios.

| No. | \bar{x} | S/N | s | S/N |
|-----|-----------|-------|------|--------|
| 1 | 91.49 | 39.23 | 3.50 | −10.88 |
| 2 | 116.61 | 41.33 | 6.23 | −15.89 |
| 3 | 148.20 | 43.42 | 9.25 | −19.32 |
| 4 | 90.53 | 39.14 | 1.39 | −2.86 |
| 5 | 113.41 | 41.09 | 2.18 | −6.77 |
| 6 | 141.40 | 43.01 | 3.14 | −9.94 |
| 7 | 86.95 | 38.79 | 1.56 | −3.86 |
| 8 | 105.15 | 40.44 | 2.51 | −7.99 |
| 9 | 131.50 | 42.38 | 3.88 | −11.78 |

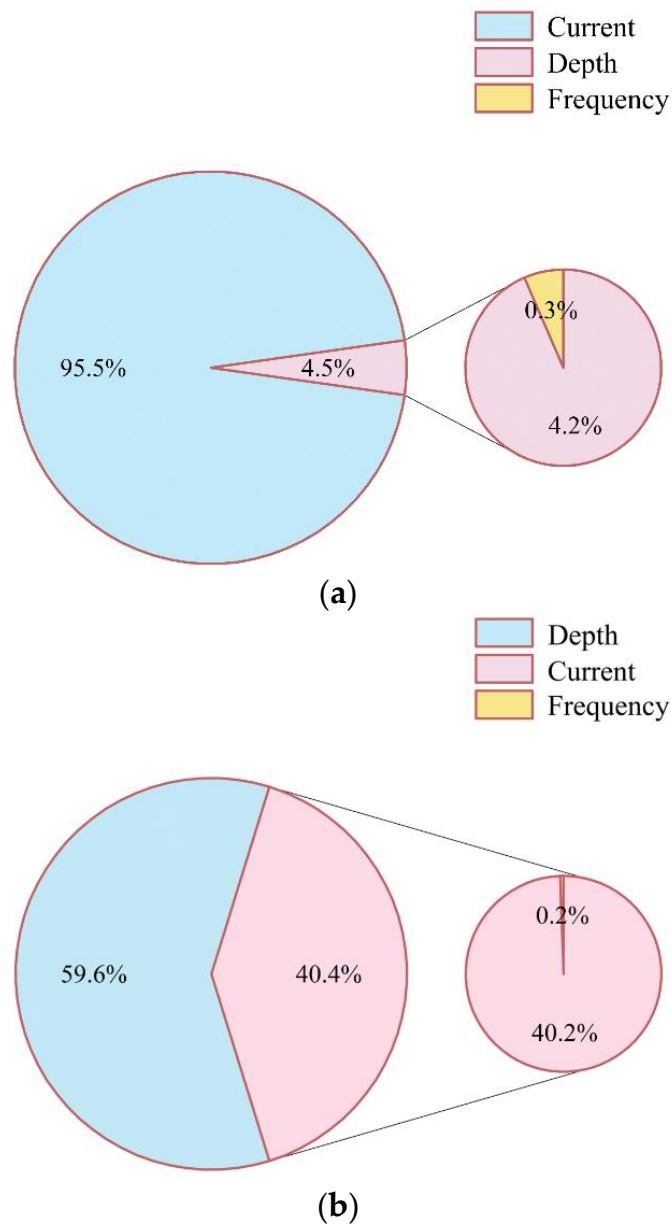


Figure 5. Percentage for the contribution rates of different factors: (a) contribution of each parameter to the max. mean temperature; (b) contribution of each parameter to temperature uniformity.

Table 6. ANOVA for max. mean temperature and temperature uniformity.

| Parameters | DF | Seq SS | Adj MS | F-Value | p-Value | Contribution |
|---|----|---------|---------|---------|---------|--------------|
| Max. mean temperature (\bar{x}) | | | | | | |
| Depth/mm | 2 | 0.9878 | 0.4939 | 30.77 | 0.031 | 4.17% |
| Current/A | 2 | 22.6452 | 11.3226 | 705.43 | 0.01 | 95.54% |
| Frequency/KHz | 2 | 0.0688 | 0.0344 | 2.14 | 0.318 | 0.29% |
| Error | 2 | 0.0321 | 0.0161 | | | |
| Totle | 8 | 23.7339 | | | | |
| Temperature uniformity (s) | | | | | | |
| Depth/mm | 2 | 136.303 | 68.1514 | 1343.91 | 0.001 | 59.59% |
| Current/A | 2 | 91.894 | 45.9469 | 906.05 | 0.001 | 40.18% |
| Frequency/KHz | 2 | 0.529 | 0.2647 | 5.22 | 0.161 | 0.23% |
| Error | 2 | 0.101 | 0.0507 | | | |
| Totle | 8 | 228.827 | | | | |

3.3. Results of Response Surface Method

The synergistic effect of any two factors on target results is analyzed by the RSM. The regression equations of the three factors on these results are formulated based on Equation (14), thus obtaining Equations (15) and (16):

$$Y_{\text{Max. mean temperature}} = 14.06 + 10.15A + 0.02234B - 0.1718C - 0.4485A^2 + 0.000078B^2 + 0.001302C^2 - 0.007136AB + 0.01805AC \quad (15)$$

$$Y_{\text{Temperature uniformity}} = 22.36 - 6.551A - 0.01150B + 0.5264C + 0.5630A^2 + 0.000013B^2 - 0.003771C^2 - 0.001142AB - 0.02700AC \quad (16)$$

In the above equations, A, B, and C are heating depth, current, and frequency, respectively. Figure 6 presents the response surface diagrams for the synergistic effect of any two parameters on target results. Therefore, (a), (b) and (c) illustrate the synergistic effects on maximum mean temperature and (d), (e) and (f) exhibit the synergistic effects on temperature uniformity. As mentioned above, the current has a much greater impact on the maximum mean temperature than the other two factors. It can also be observed from Figure 6, compared to increasing frequency, increasing current and heating depth can cause a greater temperature rise, with the current having a greater impact on the maximum mean temperature. This can also be observed from Figure 6a–c. Because frequency has less impact, it is the current or heating depth that exert more impact when they are present with frequency, which is consistent with the conclusions reached through ANOVA. Figure 6d indicates that the temperature uniformity first rises and then declines with the increase of heating depth within a certain range of current, while it decreases slightly with increased currents. Therefore, the change of this uniformity is not just a linear variation of increased or decreased heating depths and currents but the result from the interaction between them. When the heating depth is about 7 mm and the current fluctuates around 850 A, the temperature uniformity is optimal, which is in line with the conclusions drawn by Taguchi method. In Figure 6e,f is similar to (b) and (c). That is, frequency has little impact on temperature uniformity and, consequently, current and heating depth play a leading role.

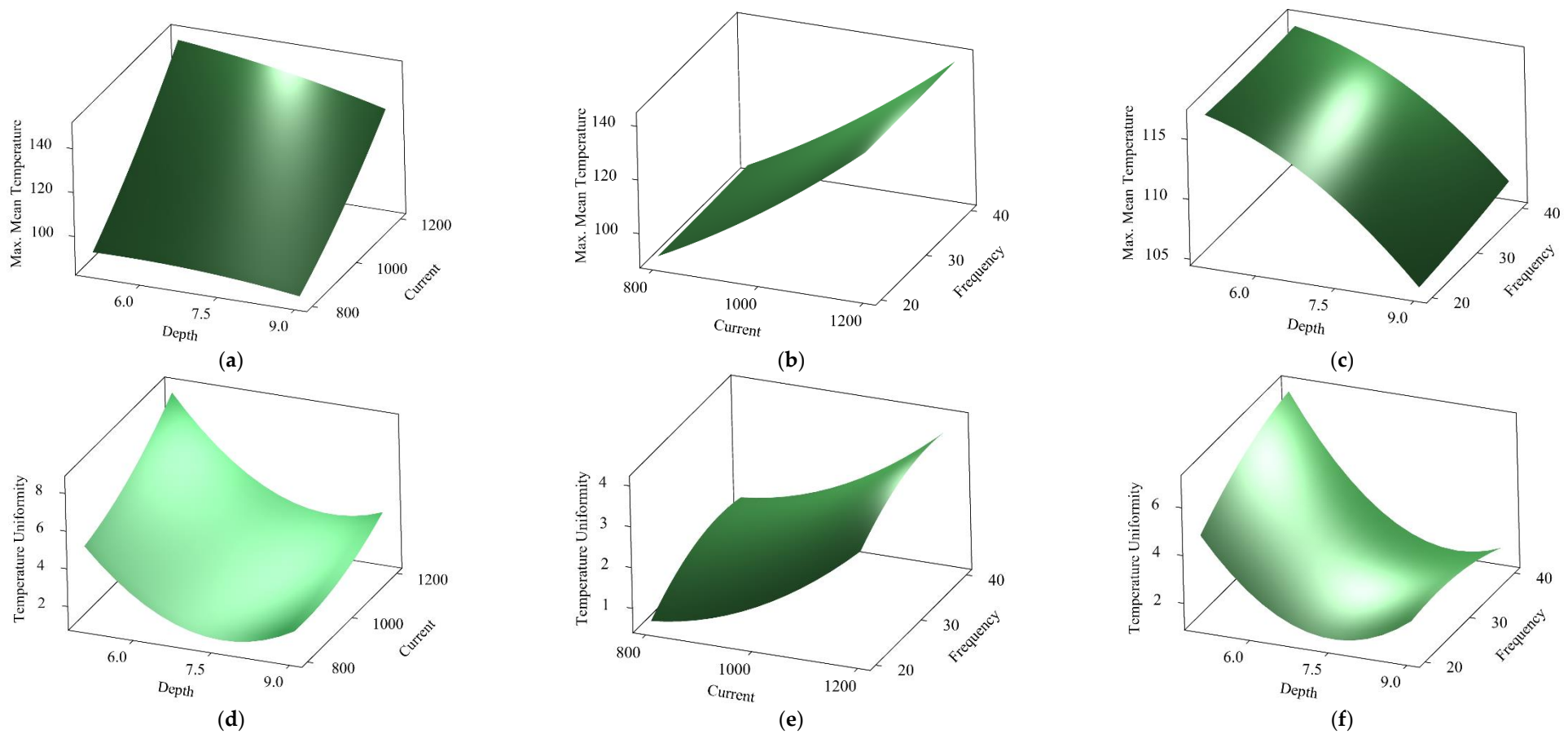


Figure 6. Response surface diagrams for the synergistic effect of different parameters on target results: (a) interaction of depth and current on max. mean temperature; (b) interaction of frequency and current on max. mean temperature; (c) interaction of depth and frequency on max. mean temperature; (d) interaction of depth and current on temperature uniformity; (e) interaction of frequency and current on temperature uniformity; (f) interaction of depth and frequency on temperature uniformity.

4. Conclusions

In this work, the temperature rise characteristics of mold induction heating were explored at different heating depths, currents, and frequencies, during which the special-shaped coils that are different from conventional spiral-shaped ones were adopted. With maximum mean temperature and temperature uniformity as target results, COMSOL Multiphysics was introduced to conduct simulation experiments. The influence of these three parameters on temperature rise characteristics on the mold surface was summarized. Results show that these characteristics do not change with different shapes of coils.

There are three factors selected by Taguchi method: heating depth, current, and frequency, each of which has three levels. On this basis, the L9 orthogonal experiment was designed to explore the extent to which each factor affects the maximum mean temperature and temperature uniformity. It can be verified that the heating depth and current have a greater impact on both target results than the frequency. Therefore, the maximum mean temperature was most affected by current, which is followed by heating depth and frequency successively, and the temperature uniformity is most affected by heating depth, which is followed by current and frequency successively. The analysis of S/N ratio indicates that in order to maximize the maximum mean temperature, the heating depth, current, and frequency shall be set at 5 mm, 1200 A, and 40 KHz, respectively. The optimal temperature uniformity was realized when the three factors are 7 mm, 800 A, and 20 KHz, respectively. Then, ANOVA was conducted on these factors to summarize their contribution rates.

Finally, the synergistic effect of any two factors on target results was discussed using RSM and the corresponding response surface diagrams were plotted. As stated earlier, frequency is involved to the least extent. Therefore, in the combination of current and frequency or heating depth and frequency, it is the former that plays a leading role. By contrast, current and frequency have similar contribution rates to temperature uniformity. Therefore, the change in this uniformity results from the interaction of these two parameters. As shown by response surface diagrams, the temperature uniformity is optimal at the current of about 850 A and the heating depth of about 7 mm, which conforms to the optimal combination obtained by Taguchi method.

Author Contributions: Conceptualization, Y.Z. and J.L.; methodology, J.L.; software, J.L.; validation, J.L., P.Z. and J.H.; formal analysis, J.L.; investigation, J.L.; resources, J.L.; data curation, J.L., P.Z. and J.H.; writing—original draft preparation, J.L.; writing—review and editing, Y.Z.; visualization, Y.Z.; supervision, Y.Z.; project administration, Y.Z.; funding acquisition, Y.Z. All authors have read and agreed to the published version of the manuscript.

Funding: This research received no external funding.

Institutional Review Board Statement: Not applicable.

Informed Consent Statement: Not applicable.

Data Availability Statement: Not applicable.

Conflicts of Interest: The authors declare no conflict of interest.

References

1. Hammami, M.; Kria, F.; Baccar, M. Numerical study of thermal control system for rapid heat cycle injection molding process. *Part E: J. Process Mech. Eng.* **2015**, *229*, 315–326. [\[CrossRef\]](#)
2. Shi, Z.; Zhang, L.; Hou, J. Review of Rapid Heat Cycle Molding Technology. *Journal of Netshape Forming Engineering. J. Netshape Form. Eng.* **2017**, *9*, 1–18.
3. Zhang, A.; Zhao, G.; Guan, Y. Effects of mold cavity temperature on surface quality and mechanical properties of nanoparticle-filled polymer in rapid heat cycle molding. *J. Appl. Polym. Sci.* **2015**, *132*, 1–9. [\[CrossRef\]](#)
4. Yang, H.; Yilmaz, G.; Han, G. A quick response and tribologically durable graphene heater for rapid heat cycle molding and its applications in injection molding. *Appl. Therm. Eng.* **2020**, *167*, 114791. [\[CrossRef\]](#)
5. Su, Q.; Zhang, N.; Gilchrist, M.D. The use of variotherm systems for microinjection molding. *J. Appl. Polym. Sci.* **2016**, *133*, 1–17. [\[CrossRef\]](#)

6. Wada, A.; Tazaki, K.; Tahara, T.; Suzuki, H.; Mizutani, Y. Injection Molded Articles with Improved Surface Characteristics, Production of Same and Apparatus Therefor. U.S. Patent US4340551 A, 20 July 1982.
7. Murata, Y.; Kanno, R. Effects of Heating and Cooling of Injection Mold Cavity Surface and Melt Flow Control on Properties of Carbon Fiber Reinforced Semi-Aromatic Polyamide Molded Products. *Polymers* **2021**, *13*, 587. [[CrossRef](#)] [[PubMed](#)]
8. Fu, X.; Chen, Q.; Chen, X.; Zhang, L.; Yang, A.; Cui, Y.; Yuan, C.; Ge, H. A Rapid Thermal Nanoimprint Apparatus through Induction Heating of Nickel Mold. *Micromachine* **2019**, *10*, 334. [[CrossRef](#)] [[PubMed](#)]
9. Muszyński, P.; Poszwa, P.; Gessner, A.; Mrozek, K. Application of Selective Induction Heating for Improvement of Mechanical Properties of Elastic Hinges. *Materials* **2021**, *14*, 2543. [[CrossRef](#)] [[PubMed](#)]
10. Poszwa, P.; Muszyński, P.; Mrozek, K.; Zielinski, M.; Gessner, A.; Kowal, M. Investigation of the Strength of Plastic Parts Improved with Selective Induction Heating. *Polymers* **2021**, *13*, 4293. [[CrossRef](#)] [[PubMed](#)]
11. Minh, P.S.; Le, M.-T. Improving the Melt Flow Length of Acrylonitrile Butadiene Styrene in Thin-Wall Injection Molding by External Induction Heating with the Assistance of a Rotation Device. *Polymers* **2021**, *13*, 2288. [[CrossRef](#)] [[PubMed](#)]
12. Omarova, A.; Yermekova, M.; Kozulina, T.P. The Numerical Simulation and Investigation of Influence of Inductor Parameters on a Quality of Induction Surface Heating. In Proceedings of the 2020 IEEE Conference of Russian Young Researchers in Electrical and Electronic Engineering, Moscow, Russia, 27–30 January 2020; pp. 795–797.
13. Thuan, H.D.; Son, T.A.; Minh, P.S. Estimate the melt flow length with internal induction heating for the injection molding process. *Key Eng. Mater.* **2020**, *863*, 97–102. [[CrossRef](#)]
14. Xiao, C.L.; Kahve, C.; Fu, C.M. Multi-objective optimization of heating system for rapid thermal cycling molding mold with internal induction heating. *SN Appl. Sci.* **2021**, *3*, 673. [[CrossRef](#)]
15. Kitayama, S.; Tamada, K.; Takano, M.; Aiba, S. Numerical optimization of process parameters in plastic injection molding for minimizing weldlines and clamping force using conformal cooling channel. *J. Manuf. Process.* **2018**, *32*, 782–790. [[CrossRef](#)]
16. Kitayama, S.; Tamada, K.; Takano, M.; Aiba, S.J. Numerical and experimental investigation on process parameters optimization in plastic injection molding for weldlines reduction and clamping force minimization. *Int. J. Adv. Manuf. Technol.* **2018**, *97*, 2087–2098. [[CrossRef](#)]
17. Nishioka, M.; Miyakawa, M. Development of Rapid Heating and Cooling Technology by Single-Mode Microwave Cavity Applied for Nanoparticle Synthesis. In Proceedings of the 2018 Asia-Pacific Microwave Conference (APMC), Kyoto, Japan, 6–9 November 2018.
18. Tamada, K.; Kitayama, S.; Takano, M.; Aiba, S. Simultaneous optimization in plastic injection molding for weldline temperature and clamping force. *Trans. JSME* **2017**, *83*, 17-00209.
19. Wang, Z. Research and Experiment of Partial Mould Thermal Field Analysis Based on Induction Heating. Master Thesis, Shanghai Jiao Tong University, Shanghai, China, 2012.
20. Kuo, C.C.; Tsai, Q.Z.; Li, D.Y.; Lin, Y.X.; Chen, W.X. Optimization of Ultrasonic Welding Process Parameters to Enhance Weld Strength of 3C Power Cases Using a Design of Experiments Approach. *Polymers* **2022**, *14*, 2388. [[CrossRef](#)] [[PubMed](#)]
21. Ryu, Y.; Sohn, J.S.; Yun, C.S.; Cha, S.W. Shrinkage and Warpage Minimization of Glass-Fiber-Reinforced Polyamide 6 Parts by Microcellular Foam Injection Molding. *Polymers* **2020**, *12*, 889. [[CrossRef](#)] [[PubMed](#)]
22. Nian, S.C.; Tsai, S.W.; Huang, M.S.; Huang, R.C.; Chen, C.H. Key parameters and optimal design of a single-layered induction coil for external rapid mold surface heating. *Int. Commun. Heat Mass Transf.* **2014**, *57*, 109–117. [[CrossRef](#)]
23. Valvez, S.; Silva, A.P.; Reis, P.N.B. Optimization of Printing Parameters to Maximize the Mechanical Properties of 3D-Printed PETG-Based Parts. *Polymers* **2022**, *14*, 2564. [[CrossRef](#)] [[PubMed](#)]

Disclaimer/Publisher’s Note: The statements, opinions and data contained in all publications are solely those of the individual author(s) and contributor(s) and not of MDPI and/or the editor(s). MDPI and/or the editor(s) disclaim responsibility for any injury to people or property resulting from any ideas, methods, instructions or products referred to in the content.